Test case n°30: Unsteady cavitation in a Venturi type section (PN)

Olivier Coutier-Delghosa, Regiane . Fortes Patella, Jean-Luc Reboud, Benoît Stutz

Test case number 30: Unsteady cavitation in a Venturi type section (PN)

By

Olivier Coutier-Delgosha, ENSTA - UER de Mécanique, 91761 Palaiseau, France
Phone: +33 (0)1 69 31 98 18, Fax: +33 (0)1 69 31 99 97, E-Mail: *coutier@enstay.ensta.fr*

Regiane Fortes-Patella, LEGI/INPG, BP 53, 38041 Grenoble cedex 9, France
Phone: +33 (0)4 76 82 50 81, Fax: +33 (0)4 76 82 50 01, E-Mail: *fortes@hmg.inpg.fr*

Jean-Luc Reboud, LEMD / UJF, BP 166, 38042 Grenoble cedex 9, France
Phone: +33 (0)4 76 88 10 78, Fax: +33 (0)4 76 88 79 45,
E-Mail: *jean-luc.reboud@grenoble.cnrs.fr*

Benoît Stutz, CETHIL/INSA, 9 rue de la Physique, 69621 Villeurbanne cedex, France
Phone: +33 (0)4 72 43 82 51, Fax: +33 (0)4 72 43 72 10,
E-Mail: *stutz@genserver.insa-lyon.fr*

1 Practical significance and interest of the test-case

A calculation of the cavitating flow field occurring in a Venturi type duct is presented in the present paper. Experimental results obtained in the same flow configuration by Stutz & Reboud (2000) are also reported. Convergent and divergent angles of the lower wall of the Venturi type section are respectively about 18° and 8° (see figure 2). According to experimental observations in this geometry the flow is characterized by unsteady cavitation behavior, with quasi-periodic fluctuations. Each cycle is composed of the following successive steps: the attached sheet cavity grows from the Venturi throat. A re-entrant jet is generated at the cavity closure and flows along the Venturi bottom toward the throat. Its interaction with the cavity surface results in the cavity break off. The generated vapor cloud is then convected by the main stream, until it collapses.

The challenge consists in simulating correctly this unsteady behavior. Two tests are proposed to evaluate the consistency of the numerical solution with the experiments:

- the evaluation of overall parameters (mean volume of vapor, standard deviation, frequency of the periodic fluctuations, phase average of the cavity shape evolution),
- the description of the flow inside the sheet of cavitation (time-averaged values and standard deviations of velocities and void fraction)

The numerical simulation of this problem requires a coupling between the Navier-Stokes equations, a model of turbulence (the Reynolds number in the proposed configuration equals 1.6 10^6), and a physical model of cavitation to predict the inception of cavitation and the behavior of the liquid/vapour mixture.

2 Definitions and physical model description

2.1 Physical model of cavitation

The present work considers a single fluid model: the fluid density ρ varies in the computational domain according to a barotropic equation of state, $\rho(P)$, that links the density to

the local static pressure (see figure 1). This equation considers that phase change occurs within a small range of pressure, ΔP_{vap}, centered on the saturation pressure P_{vap}. When the pressure in a cell is larger than $P_{vap} + \Delta P_{vap}/2$, the fluid is supposed to be pure liquid, the entire cell is occupied by liquid, and its density ρ_l is calculated by the Tait equation (Knapp *et al.* , 1970).

$$\frac{\rho}{\rho_{ref}} = \sqrt[n]{\frac{P + P_0}{P_{ref}^T + P_0}}, \tag{1}$$

where P_{ref}^T is the pressure at the domain outlet, ρ_{ref} is the liquid density, and for water, $P_0 = 3\ 10^8$ Pa and the exponent is $n = 7$. If the pressure is lower than $P_{vap} - \Delta P_{vap}/2$, the cell is full of vapor and its density ρ_v is given by the perfect gas law (isotherm approach),

$$\frac{P}{\rho} = RT, \tag{2}$$

where $R = 462$ J/K/kg for water vapor. In the other situations, the cell is occupied by a liquid/vapor mixture, which is considered as one single fluid with a variable density ρ. This one is directly related to the void fraction $\alpha = (\rho(P) - \rho_l)/(\rho_v - \rho_l)$ corresponding to the local density of the fluid.

To model the mixture state, the barotropic equation of state presents a smooth transition in the vapor pressure value neighborhood, in the range $P_{vap} \pm \Delta P_{vap}/2$. In direct relation with the range ΔP_{vap}, this equation is characterized mainly by its maximum slope $1/{C_{min}}^2$, where $C_{min}^2 = \partial P/\partial\rho$. C_{min} can thus be interpreted as the minimum speed of sound in the mixture. Its calibration was done in previous studies (Coutier-Delgosha *et al.* , 2003b). The optimal value was found to be independent of the hydrodynamic conditions, and is about 1.5 m/s for cold water (20°C), with $P_{vap} = 0.023$ bar, and corresponding to $\Delta P_{vap} \approx 0.06$ bar. These values are used here throughout the presented results.

Mass fluxes resulting from vaporization and condensation processes are treated implicitly by the barotropic state law, and no supplementary assumptions are required. Concerning the momentum fluxes, the model assumes that locally velocities are the same for liquid and for vapor: in the mixture regions vapor structures are supposed to be perfectly carried by the main flow. This hypothesis is often assessed to simulate sheet-cavity flows, in which the interface is considered to be in dynamic equilibrium (Merkle *et al.* , 1998). The momentum transfer between the phases is thus strongly linked to phase change.

2.2 Numerical resolution

To solve the time-dependant Reynolds-averaged Navier-Stokes equations associated with the barotropic equation of state presented here above, the numerical code applies, on 2D structured curvilinear-orthogonal meshes, the SIMPLE algorithm (Patankar, 1981)), modified to take into account the cavitation process. It uses an implicit method for the time-discretization, and the HLPA non-oscillatory second order convection scheme proposed by Zhu (1991). The numerical model is detailed in Coutier-Delgosha *et al.* (2003b).

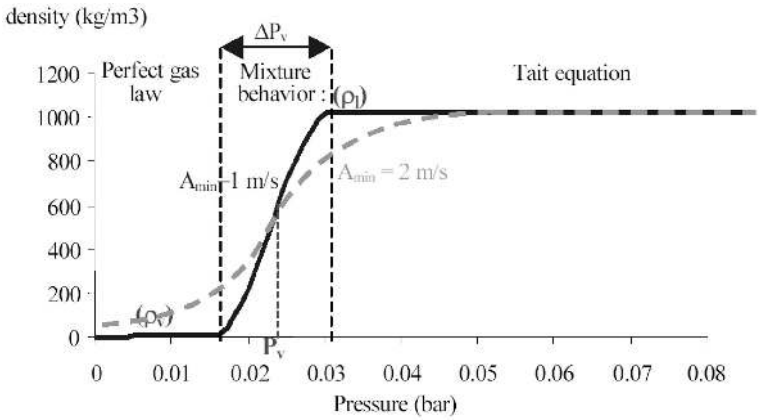

Figure 1: Barotropic state law $\rho(P)$. Water 20°C.

2.3 Turbulence model

In our previous studies (Coutier-Delgosha *et al.* , 2002, 2003b), either the k-ω model proposed by Wilcox (1998) or the k-ϵ RNG model presented by Yakhot *et al.* (1992) were applied to model cavitating flows. Results obtained have demonstrated that for both models, corrections of the influence of the vapor/liquid mixture compressibility on the turbulence should be taken into account to obtain the unsteady effects due to cavitation. For the present test case, the modified k-ϵ RNG model presented in Coutier-Delgosha *et al.* (2003a) is applied.

3 Geometry and boundary conditions

The main features of the geometry can be seen in figure 2. The precise description of the Venturi section is given as a list of coordinates for the lower wall of the Venturi (see table 1) and the upper wall of the Venturi (see table 2).

The velocity field is imposed at the computational domain inlet, and the static pressure is imposed at the outlet. Along the solid boundaries, the turbulence models are associated with laws of the wall. Details of the prescribed values are given in section 3.3.

3.1 Grid

The computational grid is composed of 160×50 orthogonal cells (figure 2). A special contraction of the mesh is applied in the main flow direction just after the throat, so that the two-phase flow area is efficiently simulated: about fifty grid points are used in this direction to model the 45 mm long mean cavity obtained by numerical calculations in the case $\sigma = 2.4$ where σ is defined in (3)(results presented hereafter). In the other direction, a contraction is also applied close to the walls, to obtain at the first grid point the non-dimensional parameter y^+ of the boundary layer varying between 30 and 100, and to use standard laws of the wall. The grid is finer in the bottom part of the Venturi section than in its upper part, to enhance the accuracy in the cavitation domain: cavities obtained contain about thirty cells across their thickness.

x (mm)	y (mm)	x (mm)	y (mm)	x (mm)	y (mm)	x (mm)	y (mm)
-152.093	0.000	13.361	14.980	61.921	8.665	151.062	-6.654
-51.706	0.000	14.508	14.833	64.027	8.376	154.938	-7.351
-42.924	2.163	15.676	14.683	66.178	8.079	158.903	-8.064
-35.553	4.558	16.869	14.531	68.396	7.770	162.936	-8.794
-29.280	6.594	18.085	14.377	70.636	7.450	167.058	-9.547
-23.971	8.324	19.326	14.218	72.921	7.117	171.269	-10.323
-19.437	9.795	20.591	14.054	75.251	6.771	175.548	-11.128
-15.589	11.045	21.881	13.889	77.626	6.411	179.894	-11.965
-12.318	12.108	23.187	13.719	80.045	6.037	184.353	-12.837
-9.538	13.011	24.531	13.540	82.510	5.647	188.878	-13.749
-7.175	13.779	25.898	13.357	85.041	5.240	193.493	-14.705
-5.166	14.432	27.309	13.180	87.595	4.818	198.198	-15.708
-3.459	14.986	28.720	12.998	90.216	4.378	202.992	-16.758
-2.007	15.458	30.177	12.805	92.882	3.923	207.876	-17.859
-0.774	15.859	31.655	12.613	95.615	3.450	212.827	-19.004
0.274	16.201	33.179	12.419	98.393	2.961	217.912	-20.188
0.509	16.298	34.724	12.220	101.216	2.456	223.065	-21.396
0.751	16.377	36.293	12.012	104.106	1.934	240.606	-24.016
0.992	16.455	37.906	11.799	107.041	1.398	258.752	-26.682
1.239	16.509	39.541	11.589	110.043	0.848	277.123	-29.392
2.143	16.395	41.199	11.379	113.089	0.283	295.717	-32.170
3.064	16.273	42.901	11.160	116.226	-0.294	314.983	-35.016
4.005	16.161	44.649	10.932	119.407	-0.881	334.474	-37.906
4.964	16.040	46.419	10.699	122.633	-1.479	354.188	-40.840
5.943	15.915	48.211	10.463	125.949	-2.085	374.575	-43.842
6.941	15.794	50.070	10.225	129.331	-2.699	395.185	-46.911
7.959	15.664	51.952	9.984	132.781	-3.328	416.244	-50.048
8.997	15.529	53.856	9.736	136.299	-3.975	437.751	-52.938
10.056	15.397	55.805	9.480	139.883	-4.632	459.929	-55.111
11.136	15.263	57.799	9.215	143.535	-5.296	1111.627	-119.228
12.238	15.123	59.838	8.945	147.254	-5.970		

Table 1: Description of the lower wall of the Venturi shown in figure 2. Coordinates must be read from top to bottom and left to right.

3.2 Initial conditions

To start unsteady calculations, the following numerical procedure is applied: first of all, a stationary step is carried out, with an outlet pressure value high enough to avoid any vapor in the whole computational domain. Then, this pressure is lowered slowly at each new time-step, down to the value corresponding to the desired cavitation number σ defined by

$$\sigma = \frac{P_{upstream} - P_{vap}}{\rho_{ref} V_{ref}^2 / 2}. \tag{3}$$

Vapor appears during the pressure decrease. The cavitation number is then kept constant throughout the computation.

x (mm)	y (mm)	x (mm)	y (mm)
-152.093	50.003	194.008	46.598
116.114	50.003	198.735	46.329
119.340	49.958	203.552	46.083
122.611	49.936	208.480	45.814
125.971	49.869	213.499	45.522
129.399	49.801	218.629	45.254
132.871	49.712	223.871	44.962
136.433	49.600	229.181	44.671
140.062	49.465	246.879	43.708
143.759	49.309	265.025	42.700
147.522	49.129	283.619	41.692
151.376	48.928	302.438	40.661
155.274	48.726	321.704	39.586
159.262	48.502	341.195	38.510
163.316	48.278	361.133	37.413
167.461	48.054	381.744	36.293
171.673	47.830	402.354	35.150
175.974	47.584	423.637	33.985
180.343	47.337	445.368	32.775
184.823	47.113	1120.140	-9.653
189.371	46.844		

Table 2: Description of the upper wall of the Venturi shown in figure 2. Coordinates must be read from top to bottom and left to right.

3.3 Calculations

Calculations are performed with non-dimensional variables based on the following reference parameters :

$\mathbf{U}_a = \mathbf{U}/U_{ref}$	U_{ref} = 7.2 m/s at the inlet
$\rho_a = \rho/\rho_{ref}$	$\rho_{ref} = \rho_{liquid}$
$C_p = (P - P_{ref})$ / $(\frac{1}{2}\rho_{ref}U_{ref}^2)$	$P_{ref} = \mathrm{P}_{outlet\ of\ the\ domain}$
$\sigma = (P_{ref} - P_{vap})$ / $(\frac{1}{2}\rho_{ref}{U_{ref}}^2)$	P_{vap} = 2000 Pa
$T_a = T/T_{ref}$	$T_{ref} = L_{ref}/U_{ref}$
	L_{ref} = chord of the Venturi = 0.224 m

Physical and numerical parameters applied:

C_{min} (minimum speed of sound in the mixture)	1.5 m/s
Re (Reynolds number based on L_{ref}, V_{ref}, and water properties)	1.6 10^6
ρ_v/ρ_l (ratio of vapor to liquid density)	0.01
Inlet turbulence level	1%
Δt (non dimensional time-step)	0.005
time order discretization	1

It is proposed to consider six flow configurations corresponding to the six cavitation numbers, σ, reported in table 3. For each calculation, the total simulation time required to eliminate the initial transient effects is at least 40 T_{ref}. The sheet of cavitation systematically adopts the oscillating behavior observed in experiments. The oscillations

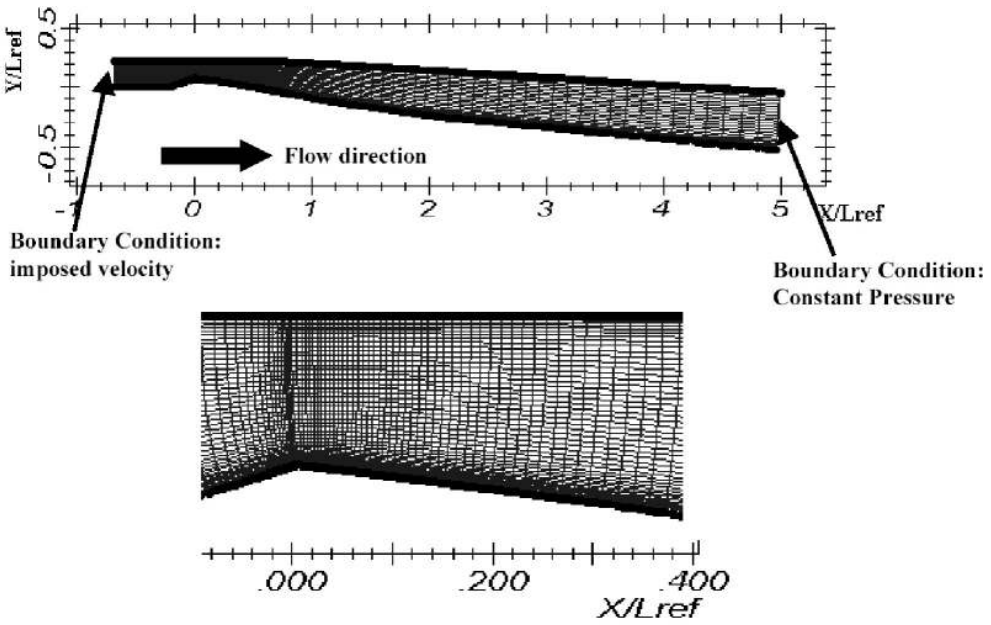

Figure 2: Curvilinear-orthogonal mesh of the Venturi type section.

are almost periodic, and their frequency as well as the mean cavity length depends on the cavitation parameter, σ.

As the final cavity obtained is fundamentally unstable, it cannot be characterized by its final shape or the final void fraction distribution. The comparisons are thus based on the transient evolution of the cavitating flow. This evolution can be defined at each time by the vapor quantity present in the domain or by the cavity shape (length, volume). We propose to focus on the vapor volume oscillations. For each computation, the time-averaged vapor volume and its standard deviation are indicated in table 3. The cavitation cycle frequency can be calculated by using a FFT analysis of the inlet pressure signal and is also given in table 3.

RESULTS			
σ	Mean vapor Volume / $L_{ref}^3 \times 10^4$	Standard deviation of the vapor volume / $L_{ref}^3 \times 10^4$	Oscillation frequency (Hz)
2.32	123	32.9	17
2.34	44.3	9.1	30
2.37	19.7	5.8	41
2.40	13.8	2.4	55
2.44	6.9	1.9	68
2.52	4.4	1.6	82

Table 3: Values of the six cavitation numbers with the corresponding results.

The transient evolution observed for σ=2.4 during the unsteady calculation is presented in figure 3. Figure 3(a) illustrates at a given time and for each cross section of the Venturi type duct the value of the minimal density present in the section. It gives information concerning the vapor cloud shedding process: the part of the cavity that breaks off clearly appears, and the fluctuation frequency can be easily calculated.

Moreover, it also shows the minimum density, *i.e.* the maximum void ratio in each section. The two other curves shown in figures 3(b) and 3(c) represent respectively the total vapor volume and the inlet pressure evolutions.

4 Comparison with experiments

4.1 Overall behavior

First, the evolution of the cavity shape at a given cavitation number is compared with pictures obtained from experiments. Two phase-averaged cavitation cycles are presented in figure 4. The right one results from experimental visualizations: Video frames acquired during a 100 ns exposure time under Laser sheet light are identified and digitized in 256 grey levels. A sampling technique is applied to classify them in nine sets corresponding to the different states of the recorded quasi-periodic pressure signal. Then, averaging the grey levels pixel per pixel for each set allows drawing a sequence of phase-averaged images, from an initial data set of 300 frames. The left part of the figure 4 corresponds to the same sequence obtained by numerical simulation (calculation duration equal to 20 T_{ref}, *i.e.* about 30 cycles). The same sampling technique is applied: the computational result is decomposed into 30×9 short sequences corresponding to the nine steps of the cavitation cycle and the phase-averaging process is applied.

From the results of table 3 concerning the effect of the cavitation number, a comparison can be proposed with results reported by Stutz & Reboud (2000): the frequency of the self-oscillation behavior is drawn with respect to the ratio V_{ref}/L_{cav}. In both the numerical simulation and the experiments L_{cav} is chosen as the maximum length of the attached cavity.

4.2 Flow field inside the sheet of cavitation

Local comparisons are proposed in the case $\sigma = 2.4$ with experimental data obtained by double optical probes measurements. This technique and the results are presented in detail in Stutz & Reboud (1997, 2000). This is an intrusive technique, which allows measurements of the local void ratio and the velocities of the two-phase structures inside the cavitation sheet. Four data profiles located respectively at $x = 1.410^{-2}$ m, 3.110^{-2} m, 4.910^{-2} m, and 6.510^{-2} m, are available. The time-averaged and standard deviation values of the velocity u and the void ratio α are compared along the four profiles in figure 6.

The three main features that should be obtained are:

- presence of the re-entrant jet, characterized by negative or zero mean values of the velocity u close to the wall.
- the rather low mean void ratio observed in the main part of the cavitation sheet: it does not exceed 25%, excepted in the upstream end of the cavity.
- the general high level of velocity and void fraction fluctuations of the same order of magnitude than the mean values.

These three characteristics of the flow are strongly related to the overall unsteady oscillation of the cavitation sheet. So an accurate numerical simulation of these features is linked to the capability of the model to predict the unsteadiness of the cavitating flow.

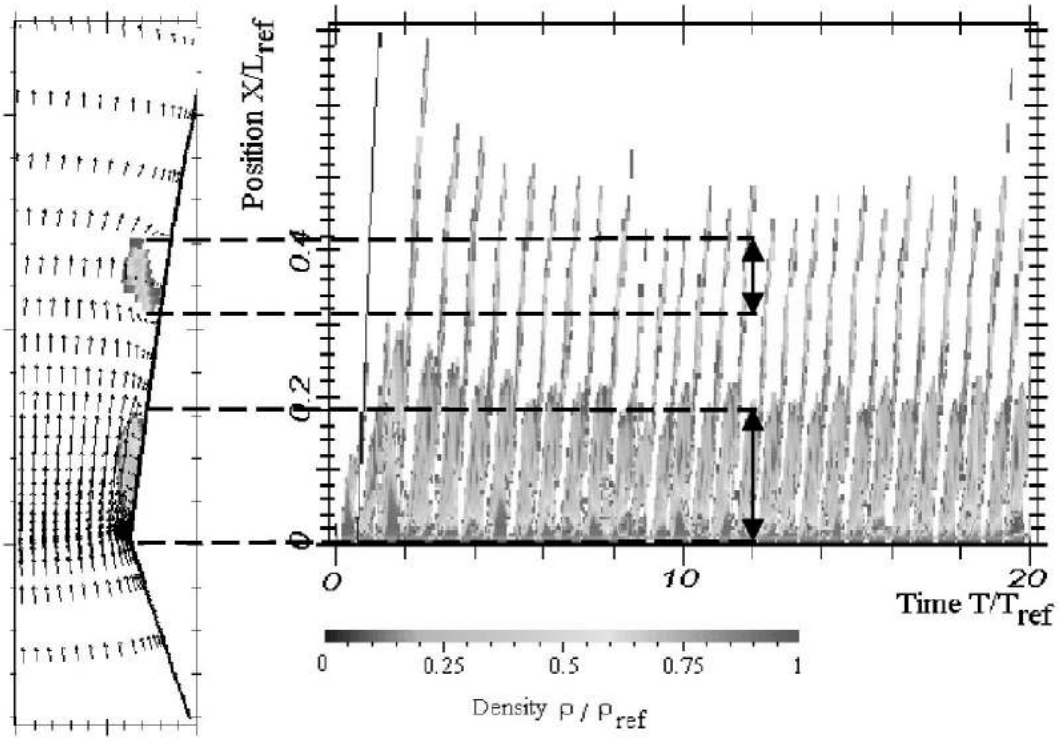

(a) Temporal evolution (in abscissa) of the cavity length (graduated in ordinate) (Instantaneous attached and cloud cavities at $T = 12T_{ref}$ are given at left)

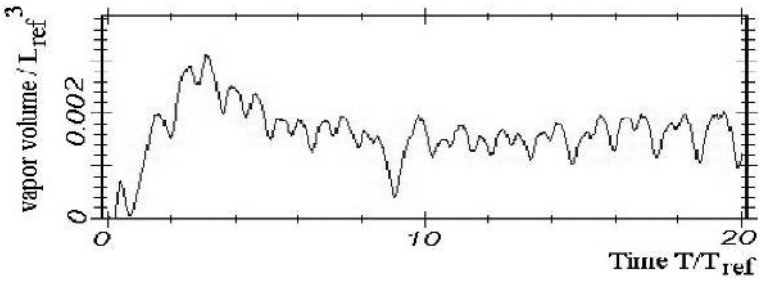

(b) Time evolution of the volume of vapor in the flow field

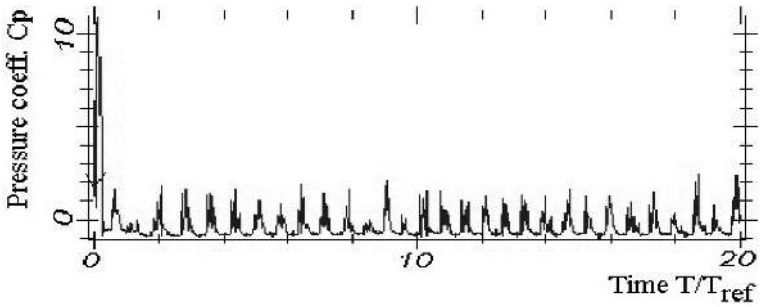

(c) Time evolution of the inlet pressure, $(P_{inlet} - P_{outlet})/\frac{1}{2}\rho_l U_{ref}^2$

Figure 3: Transient evolution of the unsteady cavitating flow in the Venturi type duct ($\sigma = 2.4$).

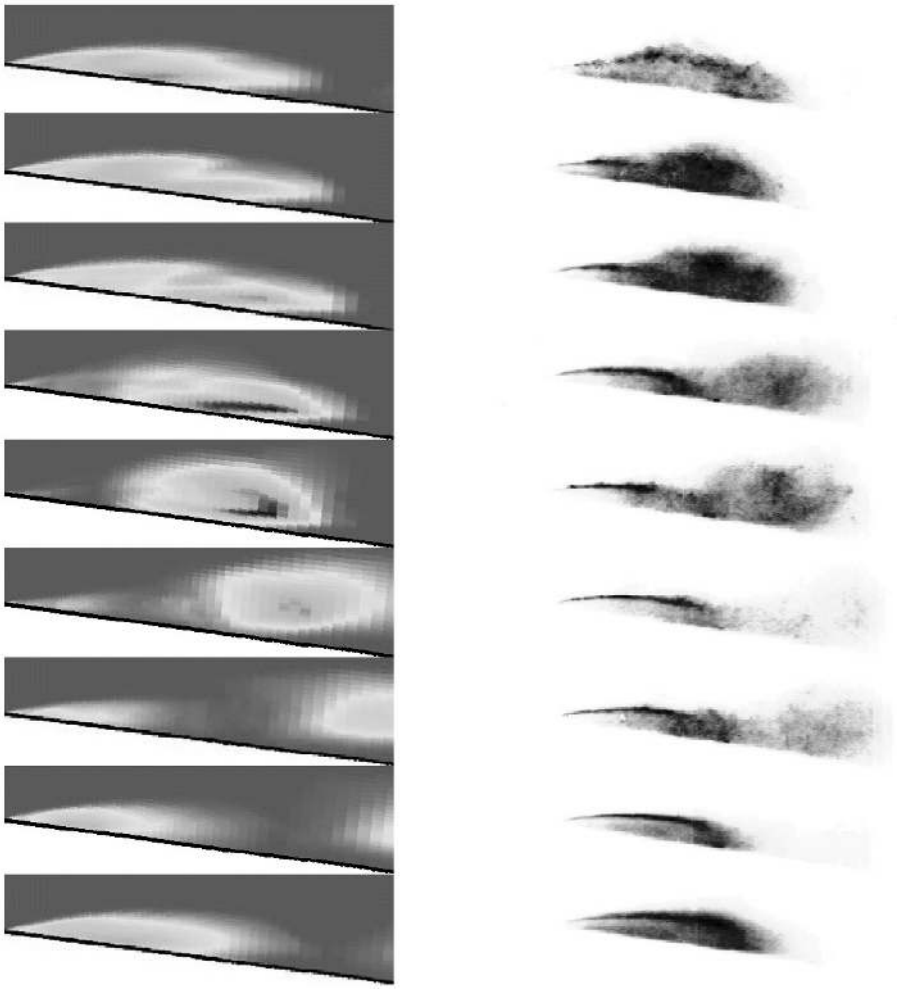

Figure 4: Numerical (on the left) and experimental (on the right) phase-averaged sequences of unsteady cavitation ($\sigma = 2.4$).

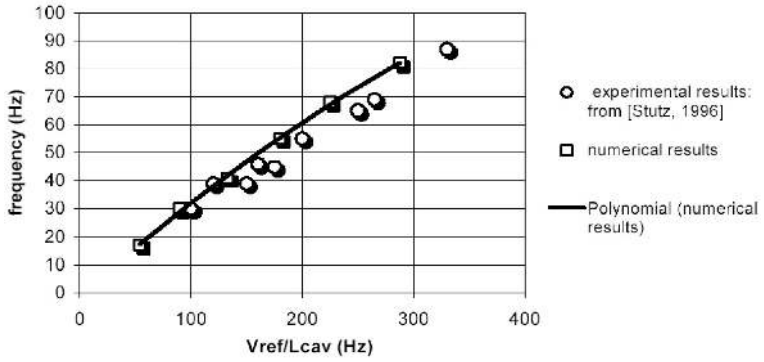

Figure 5: Experimental and numerical oscillation frequency.

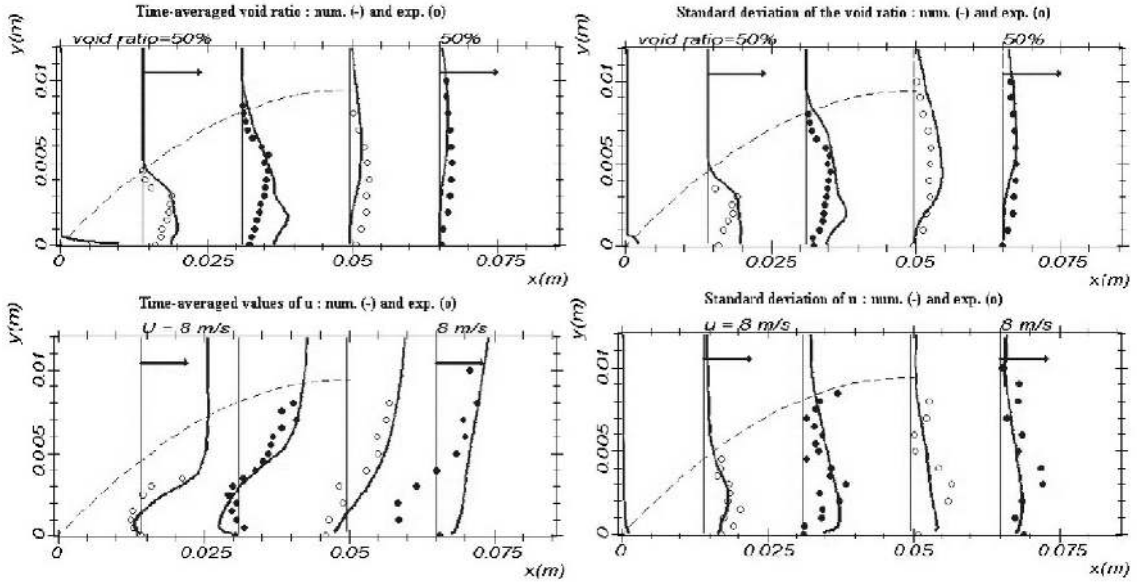

Figure 6: Time-averaged and standard deviation values of void ratio α and velocity u. Comparison between numerical results (lines) and optical probes measurements (points) for $\sigma = 2.4$. Cavity external shape in dotted line from image processing - ratio 3 between vertical and horizontal scales.

Acknowledgements

The experimental and numerical works presented in this test-case have been obtained with the continuous support of the French Space Agency (CNES). The physical model and the numerical results presented for this test case have been published by Coutier-Delgosha *et al.* (2002, 2003a) and Coutier-Delgosha *et al.* (2003b).

References

Coutier-Delgosha, O., Fortes-Patella, R., & Reboud, J. L. 2002. Simulation of unsteady cavitation with a two-equations turbulence model including compressibility effects. *J. of Turbulence*, **3**, 058. jot.iop.org.

Coutier-Delgosha, O., Fortes-Patella, R., & Reboud, J. L. 2003a. Evaluation of the turbulence model influence on the numerical simulations of unsteady cavitation. *J of Fluids Eng.*, **125**, 38–45.

Coutier-Delgosha, O., Fortes-Patella, R., & Delannoy, Y. 2003b. Numerical simulation of unsteady cavitating flow. *Int. J. for Numerical Methods in Fluids*, **42**(5), 527–548.

Knapp, R. T., Daily, J. T., & Hammit, F. G. 1970. *Cavitation.* Mc Graw Hill.

Merkle, C. L., Feng, J., & Buelow, P. E. O. 1998. Computational modeling of the dynamics of sheet cavitation. *Pages 307–314 of: Proc. of the 3rd Int. Symp. on Cavitation, Grenoble, France*, vol. 2.

Patankar, S. V. 1981. *Numerical heat transfer and fluid flow.* Hemisphere Publishing Corporation.

Stutz, B., & Reboud, J. L. 1997. Experiments on Unsteady Cavitation. *Experiments in Fluids*, **23**, 191–198.

Stutz, B., & Reboud, J.-L. 2000. Measurements within unsteady cavitation. *Experiments in Fluids*, **29**, 545–552.

Wilcox, D. 1998. *Turbulence modeling for CFD.* DCW Industries, Inc., La Canada, California, USA.

Yakhot, V., Orszag, S. A., Thangham, S., Gatski, T. B., & Speziale, C. G. 1992. Development of turbulence models for shear flows by a double expansion technique. *Phys. Fluids A*, **4**, 1510–1520.

Zhu, J. 1991. A low diffusive and oscillation-free convection scheme. *Comm. in Applied Num. Methods*, **7**, 225–232.